Macromolecules

pubs.acs.org/Macromolecules Article

Ionic Conductivity, Salt Partitioning, and Phase Separation in High-Dielectric Contrast Polyether Blends and Block Polymer Electrolytes

Congzhi Zhu,[§] Benjamin J. Pedretti,[§] Louise Kuehster, Venkat Ganesan,* Gabriel E. Sanoja,* and Nathaniel A. Lynd*

Cite This: *Macromolecules* 2023, 56, 1086−1096 Read Online

ACCESS | Metrics & More | Article Recommendations | Supporting Information

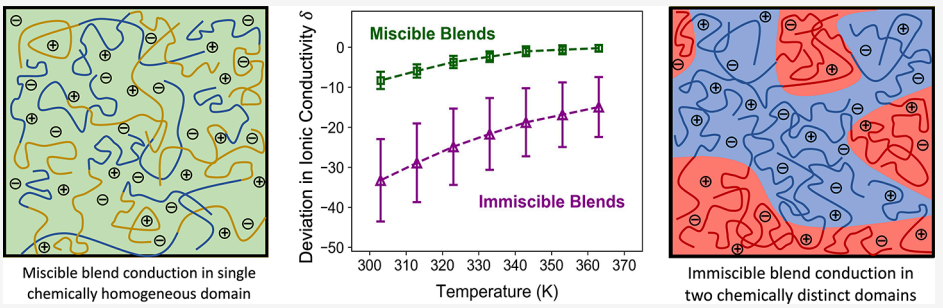

ABSTRACT: Small-molecule battery electrolytes are composed of mixtures of high-polarity and low-viscosity solvents at compositions that optimize ionic conductivity. In this work, we examined analogous polymer blends composed of one component with rapid segmental dynamics to provide low viscosity and another with a high dielectric constant (ε) to enhance ion dissociation. We investigated the inherent tradeoff between polymer polarity and segmental dynamics limiting ionic conductivity through the analysis of ionic conductivity of electrolytes containing lithium bis(trifluoromethanesulfonyl)imide (LiTFSI) with different polarity hosts: poly(allyl glycidyl ether) (PAGE) ($\varepsilon \approx 9$), poly[(cyanoethyl glycidyl ether)-*co*-(*n*-butyl glycidyl ether)] [P(CEGE-*co*-nBGE)] ($\varepsilon \approx 24$), and poly(cyanoethyl glycidyl ether) (PCEGE) ($\varepsilon \approx 36$). Two high-polarity-contrast polymer blends, PAGE/P(CEGE-*co*-nBGE)/LiTFSI and PAGE/PCEGE/LiTFSI, were prepared. While PAGE/PCEGE/LiTFSI blends were immiscible at all compositions, PAGE/P(CEGE-*co*-nBGE)/LiTFSI blends were miscible at LiTFSI concentrations above $r = 0.065$. The immiscibility of PAGE/PCEGE/LiTFSI blends imposed a negative deviation in ionic conductivity from a calculated linear average of the two single-polymer electrolytes. This negative deviation was decreased in magnitude to less than 10% in miscible PAGE/P(CEGE-*co*-nBGE)/LiTFSI blends between 30 and 90 °C. To understand the changes in the effective interaction parameter in the presence of LiTFSI, we investigated the disordered-state small-angle X-ray scattering (SAXS) of a diblock polymer, PAGE-*b*-PCEGE, across a range of LiTFSI concentrations. By fitting SAXS profiles of this copolymer using the random phase approximation and an adjustable contrast model, we found that the effective interaction parameter decreased monotonically as the LiTFSI concentration increased. At low concentrations, LiTFSI was primarily solvated in the high-polarity PCEGE-rich phase.

Downloaded via UNIV OF TEXAS AT AUSTIN on October 4, 2023 at 21:18:17 (UTC).
See https://pubs.acs.org/sharingguidelines for options on how to legitimately share published articles.

INTRODUCTION

Due to an increased deployment of intermittent renewable energy sources combined with the electrification of the transportation and chemical industries, the need has emerged for advances in materials for energy storage.[1,2] Electrolytes represent a major component in batteries, facilitating ion transport between the cathode and anode. Widely used small-molecule electrolytes (SMEs), composed of a cyclic carbonate (high-polarity component) and a linear ether or carbonate (low-viscosity component), have optimum conductivities because they balance both rapid molecular dynamics and high ion dissociation.[3,4] There is a continuing interest in replacing SMEs with nonvolatile polymer electrolytes that offer advantages in enabling new battery chemistries, mitigating dendrite growth, increasing energy density, and maximizing the transference number of the electrolyte.[5−7] However, most polymer electrolytes contain a single polymer or block copolymer with a non-conducting structural component and ion-conducting component in combination with lithium salt, in contrast with current SME blends used in lithium-ion batteries today.[8−14]

Recent work has focused on understanding the mechanism of ion transport in polymer electrolytes[8,15−18] and the structure−property relationships governing ionic conductiv-

Received: September 30, 2022
Revised: December 21, 2022
Published: January 19, 2023

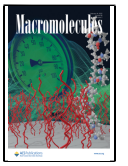

© 2023 American Chemical Society

https://doi.org/10.1021/acs.macromol.2c02023
Macromolecules 2023, 56, 1086−1096

ity.[19−23] We contributed to this research area through molecular dynamics simulations and experimental investigations of the influence of segmental dynamics and polarity of the host polymer on ion transport in polymer electrolytes.[24−29] We and others have concluded that poly(ethylene oxide) (PEO), a benchmark for polymer electrolytes, combined rapid segmental dynamics with optimized ionic solvation to enhance ionic conductivity at high temperatures (*ca.* 10^{-4} S/cm at 70 °C).[30−35] Our simulations established two polarity regimes where ion dissociation and segmental dynamics were, respectively, limiting the ionic conductivity.[25] We corroborated these simulation predictions through experimental investigations on two series of polymer electrolytes based on low-dielectric poly(vinyl ether)s and higher-dielectric poly(glycidyl ether)s. The poly(vinyl ether)-based electrolytes had glass transition temperatures (T_gs) significantly below room temperature and low dielectric constants (ε)—a measurement of polarity—in the range of 1.3 to 9.0.[28] In this low-polarity regime, ionic conductivity increased monotonically as the dielectric constant increased due to the increasing dissociation of ions in the polymer hosts. However, in our latest work on poly(glycidyl ether)s with dielectric constants in between 9.0 and 35, we revealed that a further increase in the dielectric constant of host polymers inevitably leads to stronger interchain interactions, slower segmental dynamics, and therefore decreased ionic conductivity.[29] Such an inherent tradeoff between polymer polarity and segmental dynamics limits ionic conductivity for single-polymer−host electrolytes and presents PEO as the optimal neutral polymer host for high temperature applications.

Inspired by similar tradeoffs in SMEs, we hypothesized that blending two polymers, one with rapid segmental dynamics (low viscosity) and another with high polarity (strong ionic solvation), may be a viable strategy to optimize ionic conductivity. In earlier work, we approached this problem by modeling ternary polymer−polymer−salt blend electrolytes based on coarse-grained molecular dynamics simulations.[27] Our results revealed that at moderate- to high-polarity contrast, improving the miscibility of the polymer hosts enables ionic transport in these ternary electrolyte blends.

To experimentally realize polymer blend electrolytes, it is important to develop an in-depth understanding of the lithium salt solvation in polymer blends and the influence of adding lithium salts on polymer−polymer interactions. Current experimental studies on polymer blend electrolytes and block polymers typically combine PEO with a variety of polymers as the second component.[36−39] For instance, Nakamura et al. established a thermodynamic theory to describe the solvation of ions in PEO and polystyrene (PS) blends and block copolymers.[40] Ions were solvated in PEO-rich domains due to the lack of binding moieties in PS. Gao et al. reported nontrivial miscibility changes of PEO and poly(1,3,6-trioxocane) blends with lithium bis(trifluoromethanesulfonyl)-imide (LiTFSI).[41] Recently, Shah et al. demonstrated the effect of LiTFSI addition on poly(ethylene oxide)-*b*-poly(methyl methacrylate) (PEO-*b*-PMMA) copolymers.[36] Their results provided experimental validation for the ionic self-consistent field theory developed by Olvera de la Cruz et al.[42,43] At a theoretical level, Wang et al.[40,44] and Hall and co-workers[8,15,16] calculated the thermodynamics and ion correlations in polymer blends and diblock copolymers, demonstrating preferential solvation of ions in high-polarity polymers. Brown et al. applied classical fluid density functional theory to elucidate how the microphase morphology of diblock copolymers is affected by salt.[8]

Many of the above studies are based on blends of a low dielectric constant polymer such as PS or PMMA ($\varepsilon_{PMMA} \approx 3$) with PEO ($\varepsilon_{PEO} \approx 9$), resulting in systems with low dielectric contrast ($\Delta\varepsilon = |\varepsilon_1 - \varepsilon_2| \approx 5-6$). In contrast, typical SMEs based on ethylene carbonate (EC, $\varepsilon_{EC} = 89.8$) and dimethyl carbonate (DMC, $\varepsilon_{DMC} = 3.1$) have a $\Delta\varepsilon$ of *ca.* 87. Therefore, in this study, we build upon the previous studies of polymer blends and block polymers and increase the dielectric contrast ($\Delta\varepsilon$) approaching values encountered in SME blends. Toward this objective, two blends with polarity contrasts of $\Delta\varepsilon \approx 17$ and 27 were prepared. Polymer hosts in these blends were both poly(glycidyl ether)s with a polyether backbone that can complex Li^+ ions. Although these polymers are still in the moderate polarity contrast regime when compared to the SMEs, this study probes the miscibility and ionic conductivity in the highest polarity contrast blend to date, providing system design insights that may help further optimize blend electrolytes for this application. The miscibility and the composition-dependent conductivities of these polymer blends with LiTFSI were studied. We further elucidated the change of the effective Flory−Huggins interaction parameter (χ_{eff}) in response to increased salt loadings in a high-polarity-contrast diblock polymer melt.

EXPERIMENTAL SECTION

Materials. *N*,*N*-Dibenzyl-2-aminoethanol (≥98.0%), triethylaluminum (1.0 M in hexanes), triisobutylaluminum (1.0 M in hexanes), allyl glycidyl ether (≥99%), *n*-butyl glycidyl ether (≥99%), *m*-chloroperoxybenzoic acid (70−75% stabilized with water), allyl alcohol (≥99%), acrylonitrile (≥99%), sodium hydroxide (≥97.0%), lithium bis(trifluoromethanesulfonyl)imide, and tetrahydrofuran (THF) were all purchased from commercial sources and used as received. A mono(μ-alkoxo)bis(alkylaluminum) (MOB) polymerization initiator $[(Bn)_2NCH_2CH_2(\mu_2\text{-}O)Al(iBu)_2{\cdot}Al(iBu)_3]$[45] and 2-cyanoethyl glycidyl ether (CEGE)[46] were prepared as previously described and stored under a nitrogen atmosphere.

Polymer Purification. After polymerization, the reaction vial was taken out from the N_2-filled glovebox and *ca.* 20 mL of CH_2Cl_2 was added. The vial was left on a stirrer at room temperature. After 2−5 h, the polymer was dissolved in CH_2Cl_2 to yield a homogenous solution. The polymer solution was transferred to a 50 mL Falcon tube. 1 mL of 0.1 M HCl in methanol was added, followed by the addition of 20 mL of DI water. The solution was mixed by shaking vigorously, which gave a cloudy mixture. The Falcon tube was centrifuged for 15 min at 11,000 rpm. After centrifuging, the mixture exhibited three layers. The top layer, mainly an aqueous solution, and the middle layer, a white cloudy mixture, were decanted. The above procedure was repeated for another two times with a mixture of 1 mL of 0.1 M HCl in methanol and 20 mL of DI water, followed by two times with 20 mL of DI water. The resulting clear CH_2Cl_2 solution of the polymer was transferred to a clean 20 mL scintillation vial. The solvent was removed by a rotary evaporator. The resulting viscous polymer was further dried under vacuum overnight.

Polymer Characterization. ^{1}H NMR spectroscopy was performed on a 400 MHz Agilent NMR spectrometer at room temperature and referenced to the residual solvent signal of $CDCl_3$ (7.26 ppm) or CD_2Cl_2 (5.33 ppm). Differential scanning calorimetry (DSC) was performed on a DSC250 (TA Instruments) with a RCS90 electric chiller attachment. 2.0−5.0 mg of each polymer was placed in an aluminum Tzero DSC pan with a Tzero hermetic lid. The DSC runs were conducted under a nitrogen atmosphere. The samples were first cooled from room temperature to −90 °C, then heated from −90 to 40 °C at 10 °C/min, held at 40 °C for 1 min, cooled to −90 °C at 10 °C/min, and held at −90 °C for one min. This protocol was repeated two more times but to 20 °C instead of 40 °C. The third

https://doi.org/10.1021/acs.macromol.2c02023
Macromolecules 2023, 56, 1086−1096

heating and cooling ramps were at 5 °C/min. The glass transition temperature was measured using the third heating scan. Size exclusion chromatography (SEC) was carried out on an Agilent system with a 1260 Infinity isocratic pump, degasser, and thermostatted column chamber held at 30 °C containing an Agilent PLgel 10 μm MIXED-B column with an operating range of 500−10,000,000 g/mol relative to PS standards. Chloroform was used as the mobile phase. This system was equipped with an Agilent 1260 refractometer and Infinity Bio-inert multi-detector suite featuring dual-angle static and dynamic light scattering detection. The optical microscope images were recorded under a Zeiss Axio Scope.A1 with a 20× N-Achroplan objective lens. The microscope was coupled with a Linkam LTS420 temperature-controlled stage. The samples were prepared in a nitrogen glovebox and covered with a glass coverslip.

Broadband Dielectric Spectroscopy. Dielectric constant measurements were performed with a broadband dielectric spectrometer (BDS) from Novocontrol. The instrument has a high-resolution dielectric Alpha analyzer (frequency range of 10^{-5}−10^{7} Hz) and can achieve a temperature range from −160 to 400 °C via nitrogen gas and activated heaters. The temperatures within the cell and the Alpha analyzer are controlled by WinDETA software. A parallel plate-oriented sample cell for viscous samples was used for the dielectric measurements. The viscous polymer samples were loaded on a gold-plated lower electrode with a diameter of 40 mm and covered with a smaller gold-plated electrode with a diameter of 20 mm. Teflon spacers of a known surface area and thickness were placed between the electrodes to control the thickness of the polymer sample. The measurement cell was kept closed by tightening the cell closing plate with a spring. Samples were measured from 10^{-2} to 10^{7} Hz and in a temperature range of 0 to 90 °C.

General Procedure for the Preparation of Polymer/Salt Blends. The polymers were brought into a dry nitrogen glove box and dried in vacuo below 10 mTorr at room temperature for one day. Approximately 0.2 g of polymer was added to a tared scintillation vial with a stir bar. The vial containing polymer was then dried again in vacuo overnight and reweighed. The dry weight was used to calculate how much LiTFSI would be needed. After the corresponding amount of LiTFSI was weighed and added to the vial, *ca.* 0.2 mL of anhydrous THF was added to the vial, which was then allowed to stir at room temperature for 24 h. The sample was then dried in vacuo at room temperature until it reached the weight before the solvent was added.

Electrochemical Impedance Spectroscopy. All data were collected on a BioLogic MTZ-35 Impedance Analyzer with an intermediate temperature system utilizing a through-plane conductivity cell. The electrode plates as well as the EIS chamber were brought into the glove box with a Teflon washer (surface area *ca.* 50 mm^2) with the same diameter as the electrode. The Teflon washer served to contain the polymer electrolyte and fix the distance between the electrodes. The washer was placed on one electrode, the dry polymer electrolyte was added to fill the washer, and the other electrode was placed on top and screwed in place. The electrode assembly was placed into the sample holder and sealed before being brought out of the glove box. The EIS probes and temperature probe were then inserted into the sample holder. The sample chamber was placed into an insulated temperature stage. Each experiment was run in a frequency range that encompassed the full data set at all temperatures (30 to 90 °C with a step increase of 10 °C). Impedance data were collected during both a heating cycle and a cooling cycle. The two measurements were performed for each polymer electrolyte sample. The sample was allowed to equilibrate for an hour at each temperature before data collection. The washer inner diameter and thickness was used for the sample dimensions when calculating ionic conductivity. Ionic conductivities and standard deviations were reported from the average of four data sets.

Small-Angle X-ray Scattering. All data were collected on a SAXSLabs Ganesha 300K with an X-ray wavelength of 1.5418 Å. Kapton tape and a stainless-steel washer to contain the polymer samples were brought into a nitrogen-filled glovebox. The stainless-steel washer was placed on the Kapton tape, and a polymer sample was then added to fill the washer with another piece of Kapton tape placed on top to cover the sample. The sample was sealed before being brought out of the glove box. Samples were measured in a temperature range of 30 to 80 °C with a step increase of 10 °C. Samples were allowed to equilibrate for 30 min at each temperature before data collection on heating.

RESULTS AND DISCUSSION

A high-polarity polyether with a dielectric constant higher than 20 is required in order to explore polymer−polymer miscibility and ion transport in intermediate dielectric contrast polymer blend electrolytes.[44] Poly(cyanoethyl glycidyl ether) (PCEGE) possesses polar cyano functional groups pendant to the polyether backbone that increase the overall polymer polarity. The synthesis of PCEGE was previously reported by Cantor et al. using the Vandenberg catalyst to polymerize cyanoethyl glycidyl ether (CEGE);[46] however, the resulting PCEGE was insoluble in most organic solvents and was therefore not well characterized. We hypothesized that the limited solubility of PCEGE was a result of its high molecular weight, which is typical of polymers synthesized with the Vandenberg catalyst.[47,48] Therefore, we synthesized our PCEGE using a previously reported mono(μ-alkoxo)bis(alkylaluminum) (MOB) initiator/catalyst composition that has demonstrated control over epoxide ring-opening polymerizations up to intermediate molecular weights (*ca.* 10−60 kg/mol) (Figure 1a).[45,49] The polymerization was performed to target a

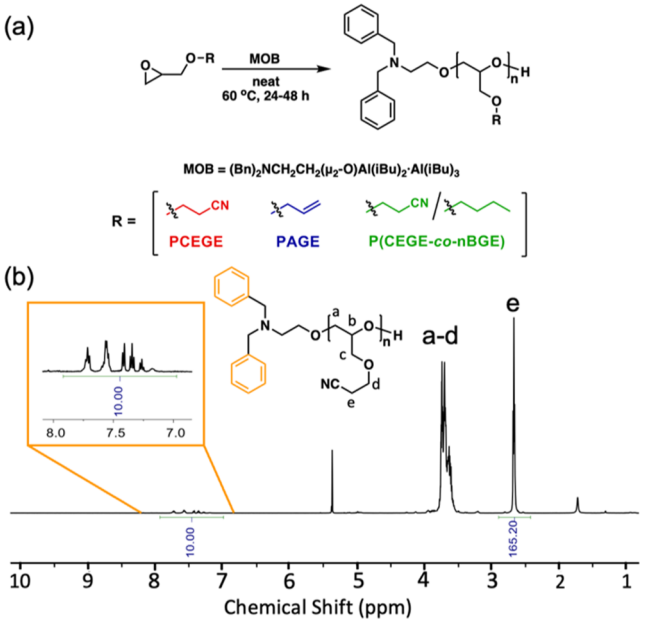

Figure 1. (a) Synthesis of PCEGE, PAGE, and P(CEGE-*co*-nBGE). (b) ^{1}H NMR spectroscopy (500 MHz) of PCEGE in CD_2Cl_2.

number-average molecular weight (M_n) of 10 kg/mol. The polymer was obtained as a viscous yellow liquid and exhibited good solubility in organic solvents such as dichloromethane, THF, and chloroform, allowing for comprehensive solution-phase characterization of its chemical structure and physical properties. M_n of PCEGE was determined via end-group analysis based on ^{1}H NMR spectroscopy (Figure 1b, Table 1) and SEC analysis relative to PS standards (Table 1). End group analysis yielded a M_n of 10.2 kg/mol and SEC analysis calculated a M_n of 10.2 kg/mol, which were close to the target of 10 kg/mol. The molecular weight dispersity ($Đ$) was

https://doi.org/10.1021/acs.macromol.2c02023
Macromolecules 2023, 56, 1086−1096

Table 1. Polymer Characterization Data

polymer	M_n[a] (kg/mol)	M_n[b] (kg/mol)	$Đ$
PAGE	11.5	10.3	1.27
P(CEGE-*co*-nBGE)	12.8	12.4	1.22
PCEGE	10.2	10.2	1.24

[a]Calculated based on end-group analysis of ^{1}H NMR spectroscopy. [b]Calculated based on GPC analysis relative to PS standards.

determined to be 1.24 by SEC relative to PS standards (Table 1). We then copolymerized CEGE with a low-polarity monomer, *n*-butyl glycidyl ether (nBGE), in a 50:50 weight ratio to synthesize a material with intermediate polarity. The resulting copolymer P(CEGE-*co*-nBGE) had M_n of 12.8 kg/mol according to end-group analysis and $Đ$ = 1.22 by SEC. For the low-polarity, low-viscosity component, we chose poly(ally glycidyl ether) (PAGE), which exhibits a polarity similar to PEO, but without semi-crystallinity.[9] PAGE/LiTFSI electrolytes have been previously investigated and exhibit conductivities of *ca.* >10^{-5} S/cm at room temperature.[9]

The dielectric permittivities of PCEGE, P(CEGE-*co*-nBGE), and PAGE were determined by broadband dielectric spectroscopy (BDS) and taken as a measurement of their polarities. The average of the plateau region of the measured real permittivity as a function of frequency was taken as the dielectric constant (ε) (Figure 2a). The dielectric permittivity

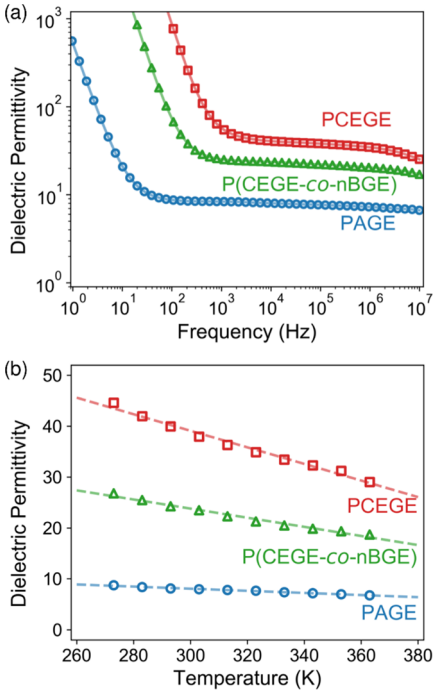

Figure 2. (a) BDS of PAGE, P(CEGE-*co*-nBGE), and PCEGE at 30 °C. (b) Dielectric permittivities of PAGE, P(CEGE-*co*-nBGE), and PCEGE in the temperature range 0 to 90 °C.

of PCEGE increased from 32 to 45 as the temperature decreased from 90 to 0 °C, which was three to four times higher than that of PAGE at all temperatures (Figure 2b), indicating the high polarity contrast between these two polymers. The dielectric permittivity of P(CEGE-*co*-nBGE) increased from 19 to 25 with decreasing temperature from 90 to 0 °C, still maintaining a high contrast with PAGE.

The glass transition temperature (T_g) is another important property that significantly affects the ionic conductivities of polymer electrolytes.[19,28,29,50−55] The strong dipole−dipole attractions between the cyano functional groups in PCEGE and P(CEGE-*co*-nBGE) results in strong polymer−polymer interactions, similar to conventional polymers like poly(acrylonitrile-*co*-butadiene).[56] Consequently, the T_gs of −37 and −56 °C, respectively, for PCEGE and P(CEGE-*co*-nBGE) were much higher than that of PAGE (−78 °C). Upon dissolving LiTFSI into the polymers, the T_g of the polymer electrolytes increased relative to the pure-polymer T_gs.

Having characterized the polarity and thermal properties of the polymers, we then investigated ion transport in electrolytes composed of binary polymer/LiTFSI blends at a concentration of r = 0.125 (r denotes the molar ratio between LiTFSI and polymer repeat units), which had previously been observed to be the optimal salt loading for PAGE homopolymers, beyond which LiTFSI solubility becomes an issue.[9] The ionic conductivities (σ) of the single-polymer electrolytes were measured with electrochemical impedance spectroscopy (EIS) under a nitrogen atmosphere. The conductivities are plotted as $\sigma(T)$ versus $1000/T$ (K^{-1}) in Figure 3a, which shows the ionic

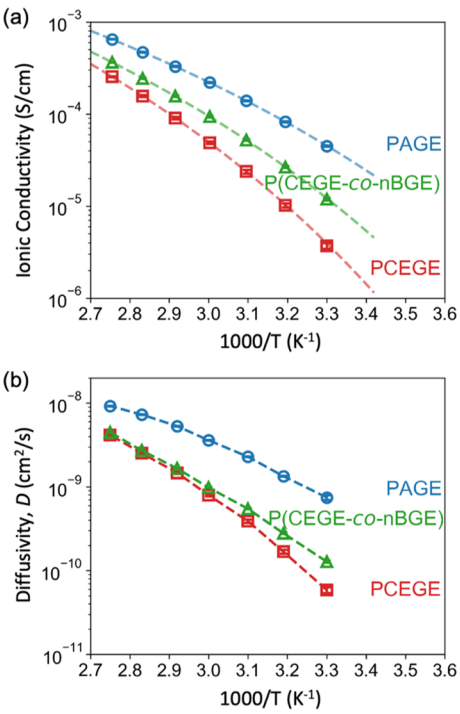

Figure 3. (a) Ionic conductivities and (b) diffusivities of PAGE-LiTFSI, P(CEGE-*co*-nBGE)-LiTFSI, and PCEGE-LiTFSI electrolytes (r = 0.125) in a temperature range from 30 to 90 °C. The dashed lines in (a) represent VTF fits to the ionic conductivity data.

conductivities measured for PCEGE/LiTFSI, P(CEGE-*co*-nBGE)/LiTFSI, and PAGE/LiTFSI blends as a function of temperature (30−90 °C). The conductivities of the PCEGE/LiTFSI electrolytes were more than 1 order of magnitude lower than those of PAGE/LiTFSI at low temperatures (≤40 °C). As the temperature increased, the conductivity of the PCEGE/LiTFSI blend increased from 10^{-6} to 10^{-4} S/cm. Such a strong temperature dependence suggested that the ionic conductivity of PCEGE was limited by segmental dynamics, which is in good agreement with our previous simulations and

https://doi.org/10.1021/acs.macromol.2c02023
Macromolecules 2023, 56, 1086−1096

experimental results in the high-dielectric permittivity regime.[29] The conductivity data were fit to the Vogel–Tammann–Fulcher (VTF) equation (eq 1), which is commonly used to model temperature-dependent conductivity in polymer electrolytes.

$$\sigma(T) = \frac{A}{T^{1/2}} \exp\left[-\frac{E_a}{R(T - T_0)}\right] \quad (1)$$

The VTF fit of experimental ionic conductivity data allows for analyzing $\sigma(T)$ as a function of temperature by qualitatively separating the effects of charge carrier concentration, often related to the prefactor A and the activation energy, E_a. In our analysis, the Vogel temperature (T_0) was included as a fitting parameter instead of being set to the typical T_g−50 value because of the possible misleading results caused by improper choice of T_0.[57] Our fitting gave T_0 close to the value of T_g−50 for the single-polymer electrolytes (see Table 2), suggesting that, in the range of temperatures investigated, the mechanism of ion conduction follows this VTF form rather than a direct Arrhenius dependence.[57]

Table 2. VTF Fitting Parameters with Variance for Single-Polymer Electrolytes with LiTFSI (r = 0.125)

	A ($K^{1/2}$·S/cm)	E_a (kJ/mol)	T_0 (K)
PAGE	5.95 ± 0.84	10.0 ± 0.4	168 ± 4
P(CEGE-*co*-nBGE)	9.28 ± 1.00	10.9 ± 0.3	179 ± 2
PCEGE	21.3 ± 3.9	12.4 ± 0.5	184 ± 3

According to the VTF analysis, the pre-factor A increased from 5.95 $K^{1/2}$·S/cm for PAGE/LiTFSI to 9.28 $K^{1/2}$·S/cm for P(CEGE-*co*-nBGE)/LiTFSI and further to 21.3 $K^{1/2}$·S/cm for PCEGE/LiTFSI. This increase in the pre-factor was consistent with the increasing polarity of the host polymer, which is expected to increase the free charge carrier concentration by increasing the solubility of LiTFSI in the polymer matrix.[25,26]

Despite the increase in charge carrier solubility in the more polar polymers, the ionic conductivities decreased with the polarity of the single-polymer electrolytes in agreement with coarse-grained molecular dynamics simulations by Wheatle et al. in the high-dielectric regime[24,25] and the corroborating experimental results.[29] Our analysis revealed that the E_a of single-polymer electrolytes increased with the polymer polarity. The higher E_a in PCEGE/LiTFSI and P(CEGE-*co*-nBGE)/LiTFSI electrolytes was attributed to stronger polymer–polymer and ion–polymer interactions, ultimately resulting in lower ion diffusivities (D). In this higher dielectric constant regime, the ionic conductivity was governed by T_g, which gives insights into relative chain mobility and not ion solubility. The observed trend in ionic conductivity was therefore expected as the T_g of the polymers increased from PAGE to P(CEGE-*co*-nBGE) to PCEGE. We calculated the diffusivities of the three single-polymer electrolytes using a method reported by Sokolov et al.[58,59] The real conductivities (σ') of PCEGE and PAGE were first plotted against frequency (ν) and then fit to the power law presented in eq 2 (Figure S33). The fitting yielded a critical frequency (ν^*) that characterizes the boundary between the DC plateau and the hopping regime and a power-law exponent (a). The diffusivity was calculated using eq 3, where n_p is the number density of charge pairs in the electrolyte.

$$\sigma(\nu) = \sigma_0\left[1 + \left(\frac{\nu}{\nu^*}\right)^a\right] \quad (2)$$

$$D = \frac{\pi\nu^*}{3}\left(\frac{3}{4\pi n_p}\right)^{2/3} \quad (3)$$

The ion diffusivities of PAGE/LiTFSI, P(CEGE-*co*-nBGE)/LiTFSI, and PCEGE/LiTFSI electrolytes increased as the temperature increased from 30 to 90 °C (Figure 3b). The diffusivity in high-polarity PCEGE/LiTFSI and P(CEGE-*co*-nBGE)/LiTFSI was significantly lower than that of PAGE/LiTFSI, particularly when the temperature was below 50 °C. Together, our results suggested that slow segmental dynamics, as characterized by a high energy barrier and limited ion diffusivity, decreased the ionic conductivity of high-polarity polymer electrolytes.

The inherent trade-off between high ion dissociation and rapid segmental dynamics makes it difficult to improve the ionic conductivity of polymer electrolytes. In other contexts, blending high-polarity and low-viscosity polymers has been studied as a strategy to overcome the transport limitations that arise in single-component polymer hosts.[41,60−63] Motivated by such studies, we examined the miscibility of 50:50 wt % PAGE/PCEGE blends as a function of LiTFSI concentration. Over the entire range of LiTFSI concentration investigated ($0 < r < 0.2$), two distinct T_gs were observed as shown in Figure 4a, suggesting the coexistence of two phases. Both T_gs increased as LiTFSI concentration increased, consistent with increasing ion concentration in both phases. The difference in T_g between phases decreased as LiTFSI concentration increased as shown in Figure 4b, but the system did not converge to a single T_g within the LiTFSI concentrations investigated. We examined the changes in T_g of PAGE/PCEGE/LiTFSI blends at a single concentration of LiTFSI (r = 0.125) while varying the composition of PAGE/PCEGE (Figure 4c). DSC traces of the entire series of the high-polarity contrast PAGE/PCEGE blends revealed two T_gs, one at *ca.* −54 °C (PAGE-rich phase) and the other at *ca.* −25 °C (PCEGE-rich phase). The T_gs of each phase in the blends were close to those of the single-polymer electrolytes. The composition of each phase was likely similar to the single-polymer electrolytes, indicating near-total immiscibility within the investigated composition range of the high dielectric-contrast PAGE/PCEGE system. The immiscibility was corroborated by optical microscopy of the blends revealing a multiphase morphology at room temperature (Figure S14).

The miscibility of lower dielectric-contrast PAGE/P(CEGE-*co*-nBGE)/LiTFSI blends was investigated in a similar manner. Varying amounts of LiTFSI were added to a symmetric polymer blend consisting of 50:50 wt % PAGE/P(CEGE-*co*-nBGE). At low LiTFSI concentration ($r < 0.04$), two glass transition temperatures were observed by DSC as shown in Figure 5a. However, when the concentration of LiTFSI was increased above r = 0.049, the blends became miscible as evidenced by a single T_g observed on the DSC. In the PAGE/P(CEGE-*co*-nBGE)/LiTFSI blends, the higher concentration of LiTFSI resulted in improved miscibility between the two polymers, eventually leading to a compatibilized polymer blend as shown in Figure 5b. At a LiTFSI concentration of r = 0.125, the PAGE/P(CEGE-*co*-nBGE)/LiTFSI blends showed a single T_g at all compositions (Figure S13) with the T_g increasing with the weight fraction of P(CEGE-*co*-nBGE) (Figure 5c). Our

https://doi.org/10.1021/acs.macromol.2c02023
Macromolecules 2023, 56, 1086−1096

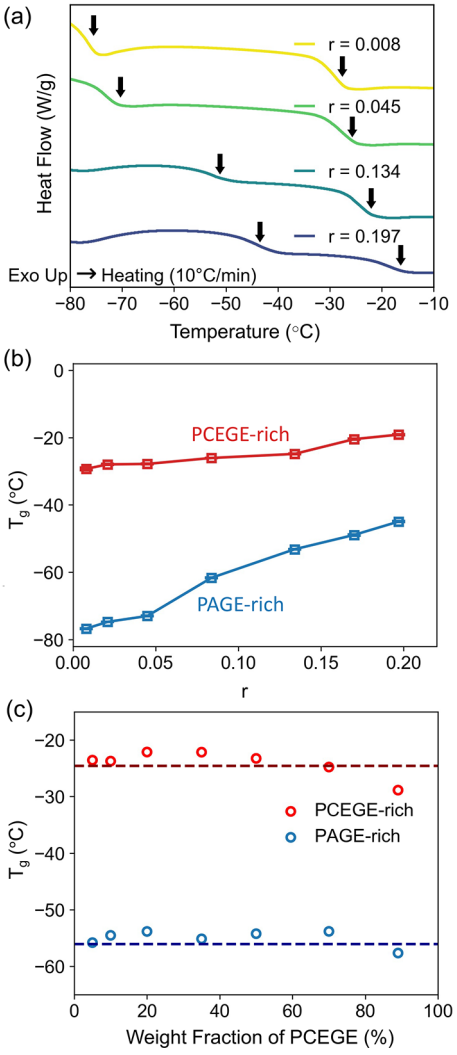

Figure 4. (a) DSC traces and (b) T_g of immiscible 50:50 wt % PAGE/PCEGE blends at different LiTFSI concentrations. (c) T_g of immiscible PAGE/PCEGE with a LiTFSI concentration of r = 0.125 at different weight fractions of PCEGE. Red/blue dashed lines represent the T_g of single-polymer electrolytes at the same LiTFSI concentration.

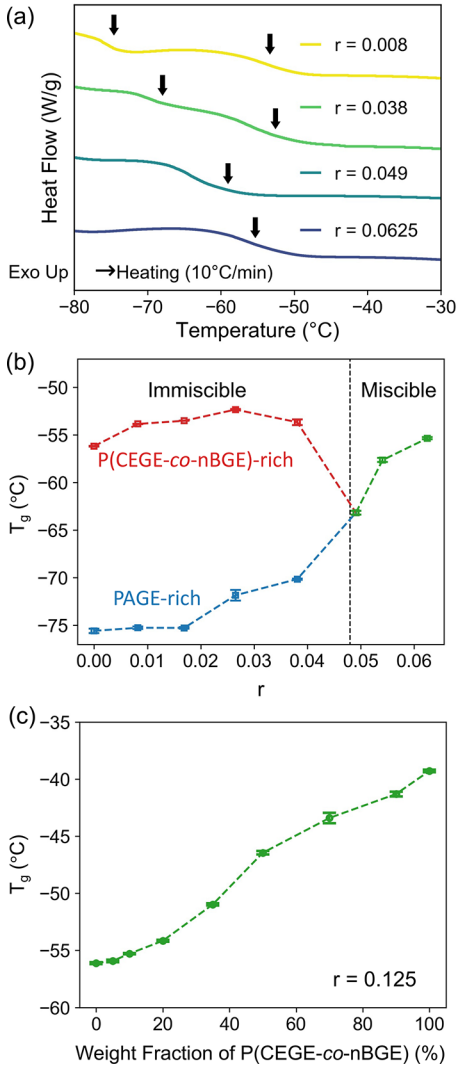

Figure 5. (a) DSC traces and (b) T_g of 50 wt % PAGE/P(CEGE-*co*-nBGE) at different LiTFSI loadings. (c) T_g of PAGE-P(CEGE-*co*-nBGE) with a LiTFSI loading of r = 0.125 at different weight fractions of P(CEGE-*co*-nBGE).

observation of the miscibility change of PAGE/P(CEGE-*co*-nBGE)/LiTFSI blends provides experimental support for a previous theoretical study that reported a decreased effective interaction parameter (χ_{eff}) in high-polarity polymer blends with added salt.[27,44]

The different behaviors of PAGE/P(CEGE-*co*-nBGE)/LiTFSI (miscible) and PAGE/PCEGE/LiTFSI (immiscible) create an opportunity to investigate how miscibility affects the ionic conductivity of polymer blends with high polarity contrast. As the composition of the high-polarity polymer in the blend increased, the ionic conductivity of the blends decreased. Wide variability was observed in the measurement of PAGE/PCEGE/LiTFSI (Figure 5a) due to its heterogeneity. To better evaluate the conductive properties of these polymer blends, the ionic conductivity of a polymer blend at a given composition and temperature ($\sigma_{blend,i}$) was compared to a conductivity model ($\sigma_{linear,i}$) calculated by assuming a linear mass-averaging of ionic conductivities of the two single-polymer electrolytes. We define the deviation (δ) as

$$\delta = \frac{1}{n}\sum_{i=1}^{n}\left(\frac{\sigma_{blend,i} - \sigma_{linear,i}}{\sigma_{linear,i}}\right) \times 100 \quad (4)$$

where n is the number of conductivity data points collected across all blend compositions for each temperature and/or salt concentration.

In previous simulations, we predicted that the deviation in ionic conductivity of high-polarity-contrast polymer blends was heavily dependent on the compatibility of the two polymers.[27] A negative δ was predicted when the two polymers did not interact with one another favorably, while positive δ was predicted when the polymer−polymer interactions were more favorable. In addition, the coarse-grained molecular dynamics simulations suggested that in compatible ternary high-polarity-contrast polymer blend electrolytes, the low-polarity, low-viscosity component increases the segmental dynamics of the high-polarity component where the ions are preferentially solvated. As such, the less negative δ of PAGE/P(CEGE-*co*-nBGE)/LiTFSI likely results from better compatibility and more favorable polymer−polymer interactions than in immiscible PAGE/PCEGE/LiTFSI (Figure 6). Above 353 K,

https://doi.org/10.1021/acs.macromol.2c02023
Macromolecules 2023, 56, 1086−1096

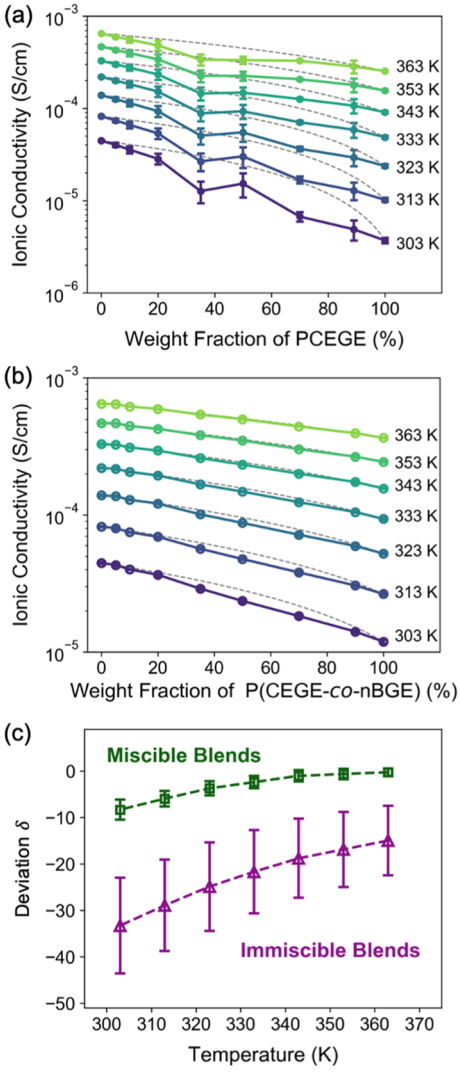

Figure 6. Ionic conductivities of (a) ternary PAGE/PCEGE/LiTFSI (r = 0.125) blends and (b) PAGE/P(CEGE-*co*-nBGE)/LiTFSI blends over a temperature range from 303 to 363 K. Dashed lines (in gray) represent the linear mass-average between the ionic conductivities of the two single-polymer electrolytes. (c) Deviation of ionic conductivities of miscible PAGE/P(CEGE-*co*-nBGE)/LiTFSI blends and immiscible PAGE/PCEGE/LiTFSI blends as a function of temperature.

the deviation is close to 0% for PAGE/P(CEGE-*co*-nBGE)/LiTFSI and the blend is miscible. This behavior contrasts with that of the PAGE/PCEGE/LiTFSI blends, which exhibit a negative δ of −15 to −33% over the entire temperature range 303−363 K due to immiscibility. However, both miscible and immiscible blends have a δ that increases with temperature, meaning that heating enhances polymer−polymer compatibility.

To investigate the relationship between polymer−polymer interactions and ion solvation in these high-polarity-contrast polymer electrolytes, we investigated the disordered state small-angle X-ray scattering (SAXS) of a model block polymer of PAGE-*b*-PCEGE, which was prepared using the same $[(Bn)_2NCH_2CH_2(\mu_2\text{-}O)Al(iBu)_2{\cdot}Al(iBu)_3]$ initiator/catalyst and sequential ring-opening polymerization of AGE followed by CEGE (Scheme 1). The resultant PAGE-*b*-PCEGE was characterized with ^{1}H NMR spectroscopy and SEC. ^{1}H DOSY NMR spectroscopy (Figure S6) demonstrated that the chain end and both blocks had the same diffusion coefficient of *ca.* 3.0×10^{-6} cm^2/s, consistent with full covalent attachment of PAGE and PCEGE blocks. Based on ^{1}H NMR, the final M_n for each block was 7.1 kDa PAGE and 13.1 kDa PCEGE.

Disordered-state SAXS profiles of PAGE-*b*-PCEGE at various LiTFSI concentrations were collected and are shown in Figure 7a at 303 K. The scattering profiles revealed a broad single peak for PAGE-*b*-PCEGE at q = 0.3−0.6 nm^{-1} at LiTFSI concentrations of r = 0.000−0.065, consistent with the disordered state of the block copolymer. The intensity of the scattering peak was sensitive to the LiTFSI concentration. The intensity first increased when a small amount (r = 0.011) of LiTFSI was added and then decreased with further addition of LiTFSI until disappearing at r = 0.113. In addition, the primary scattering peak location (q^*) for the pure diblock copolymer (r = 0.000) was at q^* = 0.451 nm^{-1} and the addition of LiTFSI (r = 0.011) resulted in a small shift to q^* = 0.458 nm^{-1} as shown in Figure 7a.

We analyzed the SAXS data within the random phase approximation (RPA) to extract the effective interaction parameter (χ_{eff}) and investigate ion-partitioning. Within this framework, the total scattering density function $I_{tot}(q)$ can be written as

$$I_{tot}(q) = I_{dis}(q) + I_{bkg}(q) \tag{5}$$

where $I_{bkg}(q)$ is the background scattering signal, which is an exponentially decaying function of q with two adjustable parameters and $I_{dis}(q)$ is the scattering profile of a disordered block polymer melt as given by[64]

$$I_{dis}(q) = C\left[\frac{S(q)}{W(q)} - 2\chi_{eff}\right] \tag{6}$$

In this equation, χ_{eff} is the effective Flory−Huggins interaction parameter, which will be different for the diblock system than the previous system containing a blend of the two homopolymers;[65] C is the X-ray scattering contrast as determined by the electron densities of the polymer phases;

Scheme 1. Synthesis of PAGE-*b*-PCEGE Diblock Copolymer Conducted Neat at 60 °C; PAGE Block Was Given 24 h to React Followed by 3 Days for the PCEGE Block

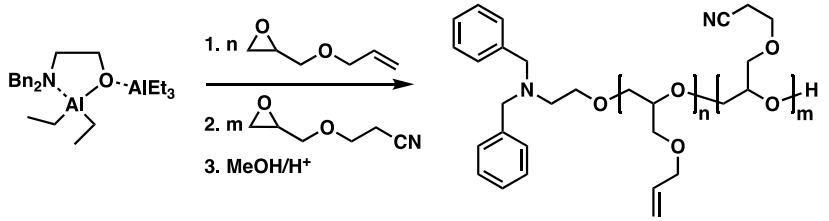

https://doi.org/10.1021/acs.macromol.2c02023
Macromolecules 2023, 56, 1086−1096

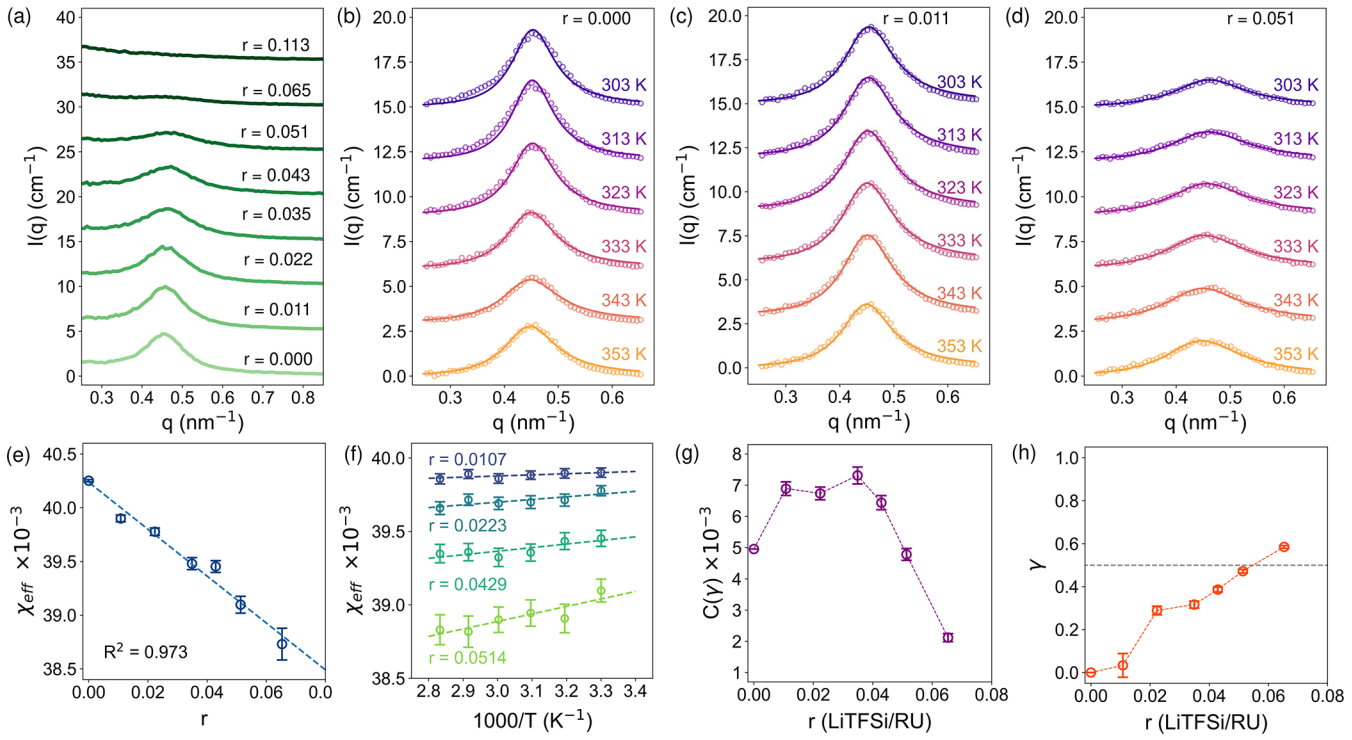

Figure 7. (a) SAXS profiles of PAGE-*b*-PCEGE with LiTFSI at various r at 303 K. Scattering profiles of PAGE-*b*-PCEGE electrolytes at different temperatures at LiTFSI concentrations of (b) r = 0.000, (c) 0.011, and (d) 0.051. The absolute scattering intensity (background subtracted) for T = 353 K is presented. Data from 343, 333, 323, 313, and 303 K are shifted vertically for clarity by 3, 6, 9, 12, and 15 cm^{-1}, respectively. The curves represent the best fit based on the adjustable contrast RPA model. (e) χ_{eff} as a function of r at 303 K. The dashed lines are linear fits of χ_{eff} and r. (f) χ_{eff} as a function of temperature at different LiTFSI concentrations. The solid lines are fits according to eq 16. (g) $C(\gamma)$ and (h) γ obtained from RPA fits with respect to increased loading of LiTFSI at 303 K.

and $S(q)$ and $W(q)$ are the determinant and the sum of the structure factor matrix as given by

$$S(q) = S_{AA}(q) + S_{BB}(q) + 2S_{AB}(q) \tag{7}$$

$$W(q) = S_{AA}(q)S_{BB}(q) - S_{AB}^2(q) \tag{8}$$

$$S_{AA}(q) = Ng(f) \tag{9}$$

$$S_{BB}(q) = Ng(1-f) \tag{10}$$

$$S_{AB}(q) = (N/2)[g(q) - g(f) - g(1-f)] \tag{11}$$

$$g(f) = (2/x^2)[fx + \exp(-fx) - 1] \tag{12}$$

$$x = q^2R_g^2 \tag{13}$$

Here, $g(f)$ is the form factor for a Gaussian chain (i.e., Debye function), and f is the volume fraction of PAGE as calculated using the density of PAGE and PCEGE and the relative composition of PAGE and PCEGE in the diblock copolymer according to ^{1}H NMR spectroscopy. N is a degree of polymerization relative to a reference volume, and R_g is the radius of gyration of the diblock copolymer.

Based on eqs 5−13, the intensity and shape of the scattering peak is determined by χ_{eff} and C, which are affected by the addition of LiTFSI to PAGE-*b*-PCEGE because of changes in microphase separation and the X-ray scattering contrast. Taking this into consideration, we adopted the adjustable contrast model developed by Balsara and co-workers to capture changes in both χ_{eff} and C.[36,66,67] In this model, C is expressed as a function of γ, a parameter that describes the preference of LiTFSI to be dissolved in either PAGE-rich (γ = 1) or PCEGE-rich domain (γ = 0).

$$C(\gamma) = \nu_{ref}\left(\frac{b_{AGE} + p(\gamma)\left(\frac{n_{LiTFSI}}{n_{AGE}}\right)b_{LiTFSI}}{\nu_{AGE} + p(\gamma)\left(\frac{n_{LiTFSI}}{n_{AGE}}\right)\nu_{LiTFSI}} - \frac{b_{CEGE} + (1-p(\gamma))\left(\frac{n_{LiTFSI}}{n_{CEGE}}\right)b_{LiTFSI}}{\nu_{CEGE} + (1-p(\gamma))\left(\frac{n_{LiTFSI}}{n_{CEGE}}\right)\nu_{LiTFSI}}\right)^2 \tag{14}$$

$$p(\gamma) = \frac{n_{AGE}(\gamma)}{n_{AGE}(\gamma) + n_{CEGE}(1-\gamma)} \tag{15}$$

In this model, b_{AGE} and b_{CEGE} are the respective X-ray scattering length densities of the polymer blocks, ν_{AGE} and ν_{CEGE} are the molar volumes of the repeat units, and ν_{ref} is the reference volume and is set to 0.1 nm^3. The important feature of this method is that the disordered scattering peak can be fitted with three adjustable parameters χ_{eff}, R_g, and γ to gain insights into the thermodynamics of ion partitioning in polymer electrolytes.

The first key observation was that the primary peak position remained relatively constant while the peak intensity decreased upon heating (Figure 7b). Similar trends were observed at higher LiTFSI concentrations (Figure 7c,d). The fit parameters varied with temperature and LiTFSI concentration. At 303 K, χ_{eff} monotonically decreases with increasing r, suggesting that LiTFSI facilitates more favorable polymer−polymer interactions between PAGE and PCEGE. The temperature depend-

https://doi.org/10.1021/acs.macromol.2c02023
Macromolecules 2023, 56, 1086−1096

ence of χ_{eff} is also shown in Figure 7f at LiTFSI concentrations of r = 0.0107, 0.0223, 0.0429, and 0.0514. The solid lines are the fits for each concentration using the empirical equation.

$$\chi_{eff} = \frac{A}{T} + B \tag{16}$$

For all LiTFSI concentrations, χ_{eff} decreased with increasing temperature, indicating better polymer miscibility at higher temperatures. This observation corroborated our earlier temperature-dependent ionic conductivity deviations from linearity (δ): For PAGE/PCEGE/LiTFSI and PAGE/P(CEGE-*co*-nBGE)/LiTFSI blends, the deviation (δ) approached zero as temperature increased. The decrease of χ_{eff} did not explain the increased scattering intensity as r was increased from 0.0 to 0.011. The plot of the X-ray scattering contrast, $C(\gamma)$, versus r (Figure 7g) shows an increase in $C(\gamma)$ from 5.1 × 10^{-3} cm^{-1} for the pure PAGE-*b*-PCEGE (r = 0.0) to 7.4 × 10^{-3} cm^{-1} at a LiTFSI concentration of r = 0.035. Further increases in LiTFSI concentration led to decreases in $C(\gamma)$. Therefore, the initial SAXS intensity increase at a low LiTFSI concentration may be attributed to the increase in contrast, $C(\gamma)$, after the addition of a small amount of LiTFSI that partitioned primarily to PCEGE-rich domains. Significantly, the adjustable contrast model was able to distinguish between simultaneous changes in χ_{eff} and $C(\gamma)$. The eventual disappearance of the primary scattering peak at r = 0.113 is attributed to both an increase in polymer compatibility as well as the decrease in scattering contrast between the two blocks.

For SMEs, a molecular-level picture of the ion solvation consists of the high-polarity component being present in the immediate solvation shell surrounding the ions.[6] Our previous molecular dynamics study on high-polarity-contrast polymer blend electrolytes with r = 0.065 also predicted that the high-polarity component is predominantly in the vicinity of solvated ions.[27] Here, when r was less than 0.05, γ was below 0.5, revealing a stronger preference for LiTFSI to be partitioned in the high-polarity PCEGE-rich domain (Figure 7h). At r = 0.011, almost all LiTFSI was solvated in the PCEGE-rich domain. As the LiTFSI concentration increased further, little selective partitioning was evident, leading to a much smaller contrast, $C(\gamma)$ (Figure 7g), and a more uniform distribution of ions in the system while χ_{eff} simultaneously decreased. The disappearance of apparent scattering peaks at high LiTFSI concentrations (c.f., Figure 7a) was attributed to the decrease in both χ_{eff} and $C(\gamma)$. To put these results in context, as with the SME blend case, the LiTFSI preferentially partitioned in the more polar PCEGE-rich phase at low concentration. Because the LiTFSI was preferentially solvated in one phase, the scattering contrast and therefore the SAXS signal intensity increased. As the amount of LiTFSI was increased, the polymer blocks became more miscible. The Li^+ ions interact with both polyethers and dilute the unfavorable segmental interactions between incompatible polymers, which explains why χ_{eff} of the system decreases. The LiTFSI compatibilized the two blocks through shared binding of Li^+ ions, decreasing the scattering contrast of the system as the LiTFSI was more uniformly distributed throughout the polymer matrix.

CONCLUSIONS

We investigated the relationship between polarity-contrast, phase behavior, and ionic conductivity in polyether blend electrolytes. PAGE/P(CEGE-*co*-nBGE)/LiTFSI was miscible at high LiTFSI concentrations, while the immiscibility of PAGE/PCEGE/LiTFSI blends gave rise to a strong negative deviation from the linear average of the ionic conductivity of PAGE/LiTFSI and PCEGE/LiTFSI. This negative deviation became less significant at higher temperature due to more favorable polymer−polymer interactions and improved miscibility. For the miscible PAGE/P(CEGE-*co*-nBGE)/LiTFSI blend electrolyte, the negative deviation in ionic conductivity was less than what was found in the immiscible PAGE/PCEGE/LiTFSI, becoming near zero when the temperature was above 353 K. This observation stresses the importance of polymer−polymer host compatibility in designing high-polarity-contrast polymer blend electrolytes. Effective polymer−polymer interactions mediated by the presence of LiTFSI were investigated by SAXS of disordered PAGE-*b*-PCEGE. We found that the effective interaction parameter decreased monotonically as the salt loading increased using the adjustable contrast model. At low concentrations, LiTFSI was primarily solvated in the high-polarity PCEGE domain as demonstrated by the low values for the partition function, γ. Future investigation into polymer blend electrolytes should focus on optimizing polarity contrast and miscibility to balance high ionic dissociation with rapid segmental dynamics and ultimately exploit a positive deviation in ionic conductivity as predicted by Wheatle et al.[27]

ASSOCIATED CONTENT

Supporting Information

The Supporting Information is available free of charge at https://pubs.acs.org/doi/10.1021/acs.macromol.2c02023.

^{1}H NMR spectroscopy, size exclusion chromatography, differential scanning calorimetry, broadband dielectric spectroscopy, and electrochemical impedance spectroscopy (PDF)

AUTHOR INFORMATION

Corresponding Authors

Venkat Ganesan − *McKetta Department of Chemical Engineering, The University of Texas at Austin, Austin, Texas 78712, United States;* orcid.org/0000-0003-3899-5843; Email: venkat@che.utexas.edu

Gabriel E. Sanoja − *McKetta Department of Chemical Engineering, The University of Texas at Austin, Austin, Texas 78712, United States;* orcid.org/0000-0001-5477-2346; Email: gesanoja@che.utexas.edu

Nathaniel A. Lynd − *McKetta Department of Chemical Engineering and Texas Materials Institute, The University of Texas at Austin, Austin, Texas 78712, United States;* orcid.org/0000-0003-3010-5068; Email: lynd@che.utexas.edu

Authors

Congzhi Zhu − *McKetta Department of Chemical Engineering, The University of Texas at Austin, Austin, Texas 78712, United States;* orcid.org/0000-0002-1302-7187

Benjamin J. Pedretti − *McKetta Department of Chemical Engineering, The University of Texas at Austin, Austin, Texas 78712, United States;* orcid.org/0000-0003-2461-822X

Louise Kuehster − *McKetta Department of Chemical Engineering, The University of Texas at Austin, Austin, Texas 78712, United States;* orcid.org/0000-0002-0730-204X

Complete contact information is available at: https://pubs.acs.org/10.1021/acs.macromol.2c02023

https://doi.org/10.1021/acs.macromol.2c02023
Macromolecules 2023, 56, 1086−1096

Author Contributions

[§]C.Z. and B.J.P. contributed equally to this work.

Notes

The authors declare no competing financial interest.

■ ACKNOWLEDGMENTS

The authors thank the Welch Foundation (F-1599 and F-1904); the National Science Foundation (CHE-2004167); and the Center for Materials for Water and Energy Systems (M-WET), an Energy Frontier Research Center funded by the U.S. Department of Energy, Office of Science, Basic Energy Sciences under Award # DE-SC0019272 (B.J.P., V.G., and N.A.L., synthesis, stipend support, and characterization).

■ REFERENCES

(1) Manthiram, A. Electrical Energy Storage: Materials Challenges and Prospects. *MRS Bull.* **2016**, *41*, 624−631.
(2) Deng, D. Li-ion Batteries: Basics, Progress, and Challenges. *Energy Sci. Eng.* **2015**, *3*, 385−418.
(3) Hall, D. S.; Self, J.; Dahn, J. R. Dielectric Constants for Quantum Chemistry and Li-Ion Batteries: Solvent Blends of Ethylene Carbonate and Ethyl Methyl Carbonate. *J. Phys. Chem. C* **2015**, *119*, 22322−22330.
(4) Ue, M.; Sasaki, Y.; Tanaka, Y.; Morita, M. *Electrolytes for Lithium and Lithium-Ion Batteries*; Jow, T. R., Xu, K., Borodin, O., Ue, M., Eds.; *Modern Aspects of Electrochemistry*; Springer: New York: NY, 2014; Vol. *58*, pp 93−165.
(5) Goodenough, J. B.; Kim, Y. Challenges for Rechargeable Li Batteries. *Chem. Mater.* **2010**, *22*, 587−603.
(6) Xu, K. Nonaqueous Liquid Electrolytes for Lithium-Based Rechargeable Batteries. *Chem. Rev.* **2004**, *104*, 4303−4418.
(7) Boz, B.; Dev, T.; Salvadori, A.; Schaefer, J. L. Review-Electrolyte and Electrode Designs for Enhanced Ion Transport Properties to Enable High Performance Lithium Batteries. *J. Electrochem. Soc.* **2021**, *168*, 090501.
(8) Brown, J. R.; Seo, Y.; Hall, L. M. Ion Correlation Effects in Salt-Doped Block Copolymers. *Phys. Rev. Lett.* **2018**, *120*, 127801.
(9) Barteau, K. P.; Wolffs, M.; Lynd, N. A.; Fredrickson, G. H.; Kramer, E. J.; Hawker, C. J. Allyl Glycidyl Ether-Based Polymer Electrolytes for Room Temperature Lithium Batteries. *Macromolecules* **2013**, *46*, 8988−8994.
(10) Chintapalli, M.; Timachova, K.; Olson, K. R.; Mecham, S. J.; Devaux, D.; DeSimone, J. M.; Balsara, N. P. Relationship between Conductivity, Ion Diffusion, and Transference Number in Perfluoropolyether Electrolytes. *Macromolecules* **2016**, *49*, 3508−3515.
(11) Young, W.-S.; Kuan, W.-F.; Epps, T. H. Block Copolymer Electrolytes for Rechargeable Lithium Batteries. *J. Polym. Sci., Part B: Polym. Phys.* **2014**, *52*, 1−16.
(12) Mindemark, J.; Lacey, M. J.; Bowden, T.; Brandell, D. Beyond PEO—Alternative Host Materials for Li + -Conducting Solid Polymer Electrolytes. *Prog. Polym. Sci.* **2018**, *81*, 114−143.
(13) Frech, R.; York, S.; Allcock, H.; Kellam, C. Ionic Transport in Polymer Electrolytes: The Essential Role of Associated Ionic Species. *Macromolecules* **2004**, *37*, 8699−8702.
(14) Nishimoto, A.; Watanabe, M.; Ikeda, Y.; Kohjiya, S. High Ionic Conductivity of New Polymer Electrolytes Based on High Molecular Weight Polyether Comb Polymers. *Electrochim. Acta* **1998**, *43*, 1177−1184.
(15) Seo, Y.; Shen, K.-H.; Brown, J. R.; Hall, L. M. Role of Solvation on Diffusion of Ions in Diblock Copolymers: Understanding the Molecular Weight Effect through Modeling. *J. Am. Chem. Soc.* **2019**, *141*, 18455−18466.
(16) Shen, K.-H.; Hall, L. M. Ion Conductivity and Correlations in Model Salt-Doped Polymers: Effects of Interaction Strength and Concentration. *Macromolecules* **2020**, *53*, 3655−3668.
(17) Hoffman, Z. J.; Shah, D. B.; Balsara, N. P. Temperature and Concentration Dependence of the Ionic Transport Properties of Poly(Ethylene Oxide) Electrolytes. *Solid State Ionics* **2021**, *370*, 115751.
(18) Choo, Y.; Halat, D. M.; Villaluenga, I.; Timachova, K.; Balsara, N. P. Diffusion and Migration in Polymer Electrolytes. *Prog. Polym. Sci.* **2020**, *103*, 101220.
(19) Schauser, N. S.; Nikolaev, A.; Richardson, P. M.; Xie, S.; Johnson, K.; Susca, E. M.; Wang, H.; Seshadri, R.; Clément, R. J.; Read de Alaniz, J.; Segalman, R. A. Glass Transition Temperature and Ion Binding Determine Conductivity and Lithium-Ion Transport in Polymer Electrolytes. *ACS Macro Lett.* **2021**, *10*, 104−109.
(20) Schauser, N. S.; Grzetic, D. J.; Tabassum, T.; Kliegle, G. A.; Le, M. L.; Susca, E. M.; Antoine, S.; Keller, T. J.; Delaney, K. T.; Han, S.; Seshadri, R.; Fredrickson, G. H.; Segalman, R. A. The Role of Backbone Polarity on Aggregation and Conduction of Ions in Polymer Electrolytes. *J. Am. Chem. Soc.* **2020**, *142*, 7055−7065.
(21) Ford, H. O.; Park, B.; Jiang, J.; Seidler, M. E.; Schaefer, J. L. Enhanced Li $^{+}$ Conduction within Single-Ion Conducting Polymer Gel Electrolytes via Reduced Cation−Polymer Interaction. *ACS Mater. Lett.* **2020**, *2*, 272−279.
(22) Liu, J.; Pickett, P. D.; Park, B.; Upadhyay, S. P.; Orski, S. V.; Schaefer, J. L. Non-Solvating, Side-Chain Polymer Electrolytes as Lithium Single-Ion Conductors: Synthesis and Ion Transport Characterization. *Polym. Chem.* **2020**, *11*, 461−471.
(23) Park, B.; Andersson, R.; Pate, S. G.; Liu, J.; O'Brien, C. P.; Hernández, G.; Mindemark, J.; Schaefer, J. L. Ion Coordination and Transport in Magnesium Polymer Electrolytes Based on Polyester-Co-Polycarbonate. *Energy Mater. Adv.* **2021**, *2021*, 1−14.
(24) Wheatle, B. K.; Keith, J. R.; Mogurampelly, S.; Lynd, N. A.; Ganesan, V. Influence of Dielectric Constant on Ionic Transport in Polyether-Based Electrolytes. *ACS Macro Lett.* **2017**, *6*, 1362−1367.
(25) Wheatle, B. K.; Lynd, N. A.; Ganesan, V. Effect of Polymer Polarity on Ion Transport: A Competition between Ion Aggregation and Polymer Segmental Dynamics. *ACS Macro Lett.* **2018**, *7*, 1149−1154.
(26) Wheatle, B. K.; Fuentes, E. F.; Lynd, N. A.; Ganesan, V. Influence of Host Polarity on Correlating Salt Concentration, Molecular Weight, and Molar Conductivity in Polymer Electrolytes. *ACS Macro Lett.* **2019**, *8*, 888−892.
(27) Wheatle, B. K.; Lynd, N. A.; Ganesan, V. Effect of Host Incompatibility and Polarity Contrast on Ion Transport in Ternary Polymer-Polymer-Salt Blend Electrolytes. *Macromolecules* **2020**, *53*, 875−884.
(28) Imbrogno, J.; Maruyama, K.; Rivers, F.; Baltzegar, J. R.; Zhang, Z.; Meyer, P. W.; Ganesan, V.; Aoshima, S.; Lynd, N. A. Relationship between Ionic Conductivity, Glass Transition Temperature, and Dielectric Constant in Poly(Vinyl Ether) Lithium Electrolytes. *ACS Macro Lett.* **2021**, *10*, 1002−1007.
(29) Pedretti, B. J.; Czarnecki, N. J.; Zhu, C.; Imbrogno, J.; Rivers, F.; Freeman, B. D.; Ganesan, V.; Lynd, N. A. Structure-Property Relationships for Polyether-Based Electrolytes in the High-Dielectric-Constant Regime. *Macromolecules* **2022**, *55*, 6730−6738.
(30) Berthier, C.; Gorecki, W.; Minier, M.; Armand, M. B.; Chabagno, J. M.; Rigaud, P. Microscopic Investigation of Ionic Conductivity in Alkali Metal Salt-Poly(Ethylene Oxide) Adducts. *Solid State Ionics* **1983**, *11*, 91−95.
(31) Webb, M. A.; Jung, Y.; Pesko, D. M.; Savoie, B. M.; Yamamoto, U.; Coates, G. W.; Balsara, N. P.; Wang, Z.-G.; Miller, T. F. Systematic Computational and Experimental Investigation of Lithium-Ion Transport Mechanisms in Polyester-Based Polymer Electrolytes. *ACS Cent. Sci.* **2015**, *1*, 198−205.
(32) Mongcopa, K. I. S.; Tyagi, M.; Mailoa, J. P.; Samsonidze, G.; Kozinsky, B.; Mullin, S. A.; Gribble, D. A.; Watanabe, H.; Balsara, N. P. Relationship between Segmental Dynamics Measured by Quasi-Elastic Neutron Scattering and Conductivity in Polymer Electrolytes. *ACS Macro Lett.* **2018**, *7*, 504−508.
(33) Fenton, D. E.; Parker, J. M.; Wright, P. V. Complexes of Alkali Metal Ions with Poly(Ethylene Oxide). *Polymer* **1973**, *14*, 589.

https://doi.org/10.1021/acs.macromol.2c02023
Macromolecules 2023, 56, 1086−1096

(34) Mao, G.; Saboungi, M.-L.; Price, D. L.; Armand, M.; Mezei, F.; Pouget, S. α-Relaxation in PEO−LiTFSI Polymer Electrolytes. *Macromolecules* **2002**, *35*, 415−419.
(35) Armand, M. Polymers with Ionic Conductivity. *Adv. Mater.* **1990**, *2*, 278−286.
(36) Shah, N. J.; Dadashi-Silab, S.; Galluzzo, M. D.; Chakraborty, S.; Loo, W. S.; Matyjaszewski, K.; Balsara, N. P. Effect of Added Salt on Disordered Poly(ethylene oxide)-Block-Poly(methyl methacrylate) Copolymer Electrolytes. *Macromolecules* **2021**, *54*, 1414−1424.
(37) Singh, M.; Odusanya, O.; Wilmes, G. M.; Eitouni, H. B.; Gomez, E. D.; Patel, A. J.; Chen, V. L.; Park, M. J.; Fragouli, P.; Iatrou, H.; Hadjichristidis, N.; Cookson, D.; Balsara, N. P. Effect of Molecular Weight on the Mechanical and Electrical Properties of Block Copolymer Electrolytes. *Macromolecules* **2007**, *40*, 4578−4585.
(38) Mullin, S. A.; Stone, G. M.; Panday, A.; Balsara, N. P. Salt Diffusion Coefficients in Block Copolymer Electrolytes. *J. Electrochem. Soc.* **2011**, *158*, A619.
(39) Panday, A.; Mullin, S.; Gomez, E. D.; Wanakule, N.; Chen, V. L.; Hexemer, A.; Pople, J.; Balsara, N. P. Effect of Molecular Weight and Salt Concentration on Conductivity of Block Copolymer Electrolytes. *Macromolecules* **2009**, *42*, 4632−4637.
(40) Nakamura, I.; Balsara, N. P.; Wang, Z.-G. Thermodynamics of Ion-Containing Polymer Blends and Block Copolymers. *Phys. Rev. Lett.* **2011**, *107*, 198301.
(41) Gao, K. W.; Loo, W. S.; Snyder, R. L.; Abel, B. A.; Choo, Y.; Lee, A.; Teixeira, S. C. M.; Garetz, B. A.; Coates, G. W.; Balsara, N. P. Miscible Polyether/Poly(ether-acetal) Electrolyte Blends. *Macromolecules* **2020**, *53*, 5728−5739.
(42) Kwon, H.-K.; Ma, B.; Olvera de la Cruz, M. Determining the Regimes of Dielectric Mismatch and Ionic Correlation Effects in Ionomer Blends. *Macromolecules* **2019**, *52*, 535−546.
(43) Sing, C. E.; Zwanikken, J. W.; Olvera de la Cruz, M. Electrostatic Control of Block Copolymer Morphology. *Nat. Mater.* **2014**, *13*, 694−698.
(44) Wang, Z.-G. Effects of Ion Solvation on the Miscibility of Binary Polymer Blends. *J. Phys. Chem. B* **2008**, *112*, 16205−16213.
(45) Rodriguez, C. G.; Ferrier, R. C.; Helenic, A.; Lynd, N. A. Ring-Opening Polymerization of Epoxides: Facile Pathway to Functional Polyethers via a Versatile Organoaluminum Initiator. *Macromolecules* **2017**, *50*, 3121−3130.
(46) Cantor, S. E.; Brindell, G. D.; Brett, T. J. Synthesis and Polymerization Studies of Cyano Epoxides. *J. Macromol. Sci., Chem.* **1973**, *7*, 1483−1508.
(47) Chwatko, M.; Lynd, N. A. Statistical Copolymerization of Epoxides and Lactones to High Molecular Weight. *Macromolecules* **2017**, *50*, 2714−2723.
(48) Vandenberg, E. J. High Polymers from Symmetrical Disubstituted Epoxides. *J. Polym. Sci.* **1960**, *47*, 489−491.
(49) Ferrier, R. C.; Imbrogno, J.; Rodriguez, C. G.; Chwatko, M.; Meyer, P. W.; Lynd, N. A. Four-Fold Increase in Epoxide Polymerization Rate with Change of Alkyl-Substitution on Mono-μ-Oxo-Dialuminum Initiators. *Polym. Chem.* **2017**, *8*, 4503−4511.
(50) Armand, M. B. Polymer Electrolytes. *Ann. Rev. Mater. Sci.* **1986**, *16*, 245−261.
(51) Armand, M. The History of Polymer Electrolytes. *Solid State Ionics* **1994**, *69*, 309−319.
(52) He, R.; Kyu, T. Effect of Plasticization on Ionic Conductivity Enhancement in Relation to Glass Transition Temperature of Crosslinked Polymer Electrolyte Membranes. *Macromolecules* **2016**, *49*, 5637−5648.
(53) Hu, H.; Yuan, W.; Jia, Z.; Baker, G. L. Ionic Liquid-Based Random Copolymers: A New Type of Polymer Electrolyte with Low Glass Transition Temperature. *RSC Adv.* **2015**, *5*, 3135−3140.
(54) Sanoja, G. E.; Schauser, N. S.; Bartels, J. M.; Evans, C. M.; Helgeson, M. E.; Seshadri, R.; Segalman, R. A. Ion Transport in Dynamic Polymer Networks Based on Metal-Ligand Coordination: Effect of Cross-Linker Concentration. *Macromolecules* **2018**, *51*, 2017−2026.
(55) Schauser, N. S.; Sanoja, G. E.; Bartels, J. M.; Jain, S. K.; Hu, J. G.; Han, S.; Walker, L. M.; Helgeson, M. E.; Seshadri, R.; Segalman, R. A. Decoupling Bulk Mechanics and Mono- and Multivalent Ion Transport in Polymers Based on Metal-Ligand Coordination. *Chem. Mater.* **2018**, *30*, 5759−5769.
(56) Hervio, V.; Bresson, B.; Brûlet, A.; Paredes, I. J.; Sahu, A.; Briand, V.; Creton, C.; Sanoja, G. E. Evolution of the Nanostructure and Viscoelastic Properties of Nitrile Rubber upon Mechanical Rejuvenation and Physical Aging. *Macromolecules* **2021**, *54*, 2828−2834.
(57) Diederichsen, K. M.; Buss, H. G.; McCloskey, B. D. The Compensation Effect in the Vogel-Tammann-Fulcher (VTF) Equation for Polymer-Based Electrolytes. *Macromolecules* **2017**, *50*, 3831−3840.
(58) Wang, Y.; Sun, C.-N.; Fan, F.; Sangoro, J. R.; Berman, M. B.; Greenbaum, S. G.; Zawodzinski, T. A.; Sokolov, A. P. Examination of Methods to Determine Free-Ion Diffusivity and Number Density from Analysis of Electrode Polarization. *Phys. Rev. E: Stat., Nonlinear, Soft Matter Phys.* **2013**, *87*, 042308.
(59) Gainaru, C.; Stacy, E. W.; Bocharova, V.; Gobet, M.; Holt, A. P.; Saito, T.; Greenbaum, S.; Sokolov, A. P. Mechanism of Conductivity Relaxation in Liquid and Polymeric Electrolytes: Direct Link between Conductivity and Diffusivity. *J. Phys. Chem. B* **2016**, *120*, 11074−11083.
(60) Wheatle, B. K.; Fuentes, E. F.; Lynd, N. A.; Ganesan, V. Design of Polymer Blend Electrolytes through a Machine Learning Approach. *Macromolecules* **2020**, *53*, 9449−9459.
(61) Kumar, K. K.; Ravi, M.; Pavani, Y.; Bhavani, S.; Sharma, A. K.; Narasimha Rao, V. V. R. Investigations on PEO/PVP/NaBr Complexed Polymer Blend Electrolytes for Electrochemical Cell Applications. *J. Membr. Sci.* **2014**, *454*, 200−211.
(62) Muthuvinayagam, M.; Gopinathan, C. Characterization of Proton Conducting Polymer Blend Electrolytes Based on PVdF-PVA. *Polymer* **2015**, *68*, 122−130.
(63) Paren, B. A.; Nguyen, N.; Ballance, V.; Hallinan, D. T.; Kennemur, J. G.; Winey, K. I. Superionic Li-Ion Transport in a Single-Ion Conducting Polymer Blend Electrolyte. *Macromolecules* **2022**, *55*, 4692.
(64) Leibler, L. Theory of Microphase Separation in Block Copolymers. *Macromolecules* **1980**, *13*, 1602−1617.
(65) Maurer, W. W.; Bates, F. S.; Lodge, T. P.; Almdal, K.; Mortensen, K.; Fredrickson, G. H. Can a Single Function for χ Account for Block Copolymer and Homopolymer Blend Phase Behavior? *J. Chem. Phys.* **1998**, *108*, 2989−3000.
(66) Chintapalli, M.; Timachova, K.; Olson, K. R.; Mecham, S. J.; DeSimone, J. M.; Balsara, N. P. Lithium Salt Distribution and Thermodynamics in Electrolytes Based on Short Perfluoropolyether-block-Poly(ethylene oxide) Copolymers. *Macromolecules* **2020**, *53*, 1142−1153.
(67) Teran, A. A.; Balsara, N. P. Thermodynamics of Block Copolymers with and without Salt. *J. Phys. Chem. B* **2014**, *118*, 4−17.

https://doi.org/10.1021/acs.macromol.2c02023
Macromolecules 2023, 56, 1086−1096